Christoph G. Rippich M.Sc. Physics

Meson Resonances Produced in the Reaction: $p+d \rightarrow He3+X^0$

Christoph G. Rippich

" Experimental Results on Meson Resonances
produced in the Reaction: $p + d \rightarrow He3 + X^{o}$ "

Department of Physics

Candidate for the degree:
Master of Science

Abstract:

The production of He3 in the reaction p+d to He3+X has been investigated at a proton beam momentum of 5 GeV/c and 12.33 GeV/c over a certain angular range. The appearance of resonant production has been studied and estimates for resonant production cross-sections have been calculated. The general features of the non-resonant production have been interpreted.

EXPERIMENTAL RESULTS ON MESON RESONANCES

PRODUCED IN THE REACTION : P + D --- HE3 + X^0.

by

Christoph G. Rippich

A thesis submitted to the Faculty of Graduate Studies and Research in partial fulfilment of the requirements for the degree of Master of Science.

Department of Physics,
McGill University,
Montreal

April 1970

Table of Contents

Acknowledgements

The author wishes to express his sincere thanks to Prof. D.G.Stairs, the director of his research, who introduced him to the High Energy Physics group at McGill University and guided him with care on his way towards research. The writer gratefully acknowledges the help of Prof. P.M.Patel who gave him the basic introduction into the fields of physics , connected to the experiment described herein.

The considerable assistance of Prof. D.G.Ryan rendered in discussions about the data analysis and the interpretation of the results, is greatly appreciated.

The author is also indebted to Prof. J.Trischuk for his help in obtaining the large amount of technical data concerning the experiment. Special thanks are extended to Dr. F.Sannes (now at Rutgers University) for his assistance in the understanding of the sophisticated electronic equipment.

The work of the author was financially supported with a research fund granted by the Foster Radiation Laboratory, which is gratefully recognized.

THE EXPERIMENT

1. Introduction

The experiment described herein was performed from May 1969 till September 1969 at the Argonne National Laboratory. It was a pure counter experiment, measuring the He3 production rate from the reaction $p + d \longrightarrow He3 + (\text{missing mass})$. The purpose of the experiment was to investigate the He3 production cross-sections for a missing mass (M.M.) region of 0.5...1.3 GeV/c^2 and 1.8...3.0 GeV/c^2 and to see if any structure in the M.M. spectra is detectable, indicating possible meson resonances. The general layout can be seen in fig.1 & 2.

For reasons of high counting rates and good resolution, the Jacobian Peak method was being used, as described in sect.3 . Identification of the emitted He3 was done by pulse height selection and time-of-flight measurement between the counters T_0,T_1, and T_2. The reaction kinematics are completely defined, including the determination of the M.M. value, by measuring the angle and momentum of the He3 particles at a given beam energy. Angular and momentum acceptances are defined by

a collimator inside the magnet and by the geometries of the trigger system T_0, T_1, T_2.

The magnet deflected the He3 by 28° upwards into the trigger system, thus decoupling the measurement of the emission angle from the momentum. Very convenient were the focussing properties of the magnet in the plane perpendicular to the bending plane, allowing to obtain the angle of emission at the target from the response of a certain element out of a seventy element scintillation counter hodoscope placed at the focal plane of the magnet (see sect.4 & 6).

As indicated in fig.2, the magnet could be rotated vertically and the target shifted along the beam line together with a shift of a movable rack, on which the hodoscope and the counters T_1 and T_2 had been mounted, to give a total sweep of the He3 production angle from 20 to 40 degrees.

Using the setup with a proton beam from the External Proton Beam Line II at the ZGS, at an incident beam momentum of 12.33 GeV/c or 5.0 GeV/c , the He3 production rate has been measured in an angular range from 25° to 35°, and resonant as well as non-resonant differential cross-sections for production of missing masses in the range from 0.5...1.3 GeV/c^2 at p_i=5 GeV/c and from

1.8...3.0 GeV/c^2 at p_i = 12.33 GeV/c have been calculated. It is the aim of this work to show how the data had been taken and were evaluated.

2. Some Remarks on the Motivation of the Experiment

Within the last few years, physicists have become increasingly aware of the necessity to obtain data with good statistics about the possible existence of boson resonances with high mass values. The basic and so far most complete work in this direction for non-strange mesons has been done by a group at CERN[1] which used a missing mass spectrometer for the reaction $\pi^{\pm}+p \longrightarrow p+MM$. One of the many famous results is the strong evidence for a split A_2 meson, and the discussions about a satisfactory explanation of this fact are only starting. (Since then, also strange mesonic resonances have been investigated in reactions of the type $K^{\pm}+N \longrightarrow N+MM$.) The non-strange resonances have been surveyed up to a mass region of ~ 2.5 GeV/c^2, but the results for $Mc^2 \gtrsim 2.0$ GeV are still in doubt: Peculiarities in cross-section spectra are referred to merely as "bumps" or "structures" under careful avoidance of the term "resonances"[2]. Hence, the reaction $p + d \longrightarrow He3 + MM$. at $p_{inc}=12.33$ GeV/c has been proposed with the following aims:

a) to increase statistics in the range below 2.5 GeV/c^2, and

b) to gather new data for mass values up to 3.5 GeV/c^2.

The last point is in fact the main motivation:

It is of great importance to study the behaviour of the Regge trajectories for high mass values. So far, the resonances A_2, R, S, T, and U (for convenience only, I will use the term "resonance" throughout) seem to follow a straight line if plotted in a diagram "peak number" versus squared mass; the peak number is identical to the spin if the latter could be established, and then the line represents a trajectory. If this behaviour continues, then the separation between the mass values of the resonances will decrease, and the widths will have to get narrower[3,4]. This effect, if present, should become noticeable at around 3.0 GeV/c^2 and would present some problems in view of the Regge theory: In general, the imaginary part of any trajectory $\alpha(t)$ is expected to increase with t, hence the widths are expected to increase, which is possible only for a deviation of the mass^2 - peak number - curve from the straight line. This opposite effect, if present, would appear also at roughly 3.0 GeV/c^2.

It should be possible to obtain some evidence about these effects by studying the reaction p + d $\longrightarrow$ He3 + MM. There are several points in favour for this reaction:
i) He3 can be identified in a relatively easy way (sect.4&5).
ii) Isospin is restricted to the values 0 and 1, which allows to assign a definite isospin I=1 to the R, S, T, and U

mesons in case they show up, because it is known that they have an isospin $I \geqq 1$ [2].

iii) The dominant vertex for p + d ⟶ He3 + MM is expected to be of the type

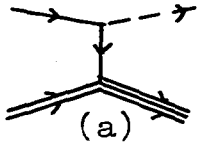

compared to

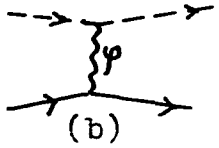

for π + N ⟶ N + MM.

In (b), the resonance producing vertex involves the coupling to an exchanged meson φ, and dependent on the nature of φ, it is possible that some resonances MM. are very much suppressed. If for instance a ρ-meson is exchanged, production of a ϕ(1019) is very low, as the ϕ has a very small width.

In (a), however, the nucleon - antinucleon vertex is open to all channels; consequently: if resonances are being produced by (a), they should appear in a larger number in (a) than in (b) for I=0 or 1.

Graphs showing the boson spectrum and the peak number plot as present at the time that the experiment p + d ⟶ He3 + MM was performed, are given in fig. 3 and 4.

3. The Jacobian Peak Method

The effect employed in the Jacobian Peak method is a wellknown fact from relativistic (and non-relativistic) kinematics : under certain circumstances, the angle at which one of the two outgoing particles in an inelastic two-body-collision is emitted may not exceed - in the laboratory coordinate system - a certain maximum angle, which depends only on the particular mass values and the incident momentum.

Let m_i, $\vec{p}_i$, E_i, p_i be the masses, momenta, energies, and 4-momentum-vectors involved in the reaction

$$1 + 2 \longrightarrow 3 + 4 \ .$$

Furthermore, the subscripts L and C shall designate variables as given in the laboratory and the CMS system, respectively:

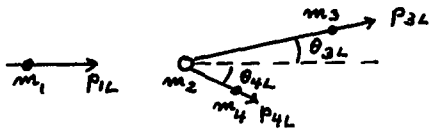

LAB

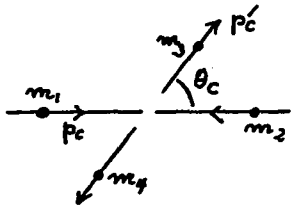

CMS

Applying the Lorentz transformation between the two systems, we get a relation between the angles (for a derivation of the following formulae, see app.1) :

$$\text{tg}\,\theta_{3L} = \sin\theta_C \,/\gamma\, x\,(\cos\theta_C + \rho_3)$$

(1)

$$\text{tg}\,\theta_{4L} = \sin\theta_C \,/\gamma\, x\,(-\cos\theta_C + \rho_4)$$

with $\beta = p_{1L} / (E_{1L} + m_2)$ = velocity of the CMS and $\gamma = 1/\sqrt{1-\beta^2}$, and

$\rho_{3(4)} = \beta \times E_{3(4)C} / p_{3(4)C} = \beta / v_{3(4)C}$.

Then θ_{3L} will assume a maximum with respect to θ_C if $\cos\theta_C = -1/\rho_3$, which shows up the almost natural condition that $\rho_3 > 1$, i.e. $v_{3C} < \beta$.

If particle 4 represents the effective mass of a multi-particle system, then the continuously variable mass m_4 is a unique function of either p_{3L} or θ_{3L} at the Jacobian peak.

The analytical expressions are:

$$t_{JP} = -s + m_1^2 + m_4^2 + 2m_3^2 \times \frac{s - m_1^2 + m_2^2}{s + m_3^2 - m_4^2}$$

(2)

$$\cos\theta_{C,JP} = (-)\,\frac{s + m_2^2 - m_1^2}{s + m_3^2 - m_4^2} \times \sqrt{\frac{\lambda(s,m_3^2,m_4^2)}{\lambda(s,m_1^2,m_2^2)}}$$

with $t = (p_3 - p_1)^2$ and $s = (p_1 + p_2)^2$, and $\lambda(a,b,c) = a^2+b^2+c^2-2ab-2ac-2bc$. The maximum angle

of Θ_{3L} , $\Theta_{3L,JP}$, is obtained by inserting (2) in (1).

These formulae also show that there exists an angle Θ_{3L} beyond which m_3 may not appear under any circumstances: $\Theta_{3L,max.} = \Theta_{3L,JP,(m_4=0)}$, for instance in the reaction of the experiment, $\Theta_{3L,max.} = 38^{o}13'$ for $p_{inc.} = 12.33$ GeV/c .

For the reaction p + d ---→ He3 + M.M., the kinematics in the lab.-frame are displayed in fig.5 for various values of the effective mass.

Two short remarks on the formulae shall be made:

a) all $\Theta_{C,JP}$ lie between 90^{o} and 180^{o} ,

b) from $\partial m_4/\partial p_{3L}(\Theta_3=\text{const}) = (-)\dfrac{\partial\Theta_3/\partial p_{3L}(m_4=\text{const})}{\partial\Theta_3/\partial m_4(p_{3L}=\text{const})}$

(3) one gets: $\partial m_4/\partial p_{3L}(\Theta_3=\text{const}=\Theta_{3L,JP}) = 0.$

The Jacobian Peak method is quite usefully applied[5] in evaluating an effective mass spectrum of a reaction of the type (I): a + b ---→ c + X.

The assumptions entering are:

i)The production of the non-resonant background in (I) varies only slowly with Θ_{3C} and p'_C at - as well as off - the Jacobian peak angle.

ii)Any resonances produced in (I) should have small widths in order to make full use of the J.P. method.

The advantages are:

i)At the J.P., the effective mass is a function of $\theta_{3L,JP}$ only at fixed incident momentum - equ.(2).

ii)The results of the mass spectrum become independent of the accuracy with which p_{3L} is measured - equ.(3).

iii)At the J.P., $d\Omega_{3L}/d\Omega_C = 0$, and therefore counting rates are strongly enhanced: With a small angular bite $\Delta\theta_{3L}$ it is possible to cover several degrees in the CMS system.

iv)Most resonance producing reactions of type (I) are peripheral processes which favor forward production of $X^{(5)}$. Thus θ_{3C} is distributed mainly between 90° and 180°, encreasing the effect of the J.P.method strongly.

v)All these advantages become especially useful in the case of counter experiments, as then the crucial condition of a small bite $\Delta\theta_{3L}$ is mostly fulfilled.

4. Instrumental Details

The Beam:

The time structure of the external proton beam at the ZGS is given in fig.6 . The momentum was 12.33 GeV/c with a spread of $\pm$ 4 MeV/c (HWHM) and a stability of the nominal value of $\lesssim 0.05\%$. The beam spot at the target had a diameter in the range of $\lesssim 0.5"$(FWHM); the spot size was nearly independent of the position of the target because the beam came to a focus at some twenty feet behind the target. The phase space area was $\lesssim 0.5\pi$ mrad-inches(FWHM) both vertically and horizontally. Hence we get an angular spread $\Delta\theta$ due to the beam emittance of ~ 1.0 mrad(FWHM), which shall be called $\Delta\theta_b$.

Rates were available in the range of 2×10^{11} protons per spill. Three beam rate monitors were being used: An absolute one provided by ZGS, giving the beam intensity directly in protons per burst, and two relative ones which had to be calibrated against the ZGS-monitor. The location of these two monitors may be seen in fig.2 . They used a thin slab of lucite and a thin mylar foil as scattering targets. For calculations of cross sections, these two relative monitors had to be used, as the ZGS monitor could not be gated by our electronics. For further details on the monitors, see sect.6 .

For a short period of time, proton momenta of 5 GeV/c were available using a "front porch" extracted beam (fig.6). In this case, however, the angular spread was much larger, and a tapered collimator in front of the target was necessary. This made the determination of absolute cross sections impossible. Only orders of magnitude could be obtained.

The Target:

A schematic view of the target may be seen in fig.7 . It consisted of a mylar cylinder of 24" length and 2" diameter contained in a vacuum chamber. The whole target setup could be moved along the beam line by ± 4 feet in order to cover the desired angular range. The liquid-gas-system was completely closed so that, once a main reservoir was filled with pure liquid deuterium, the liquid in the target was - and stayed - practically free of any contaminations. The target could be emptied by allowing vapor pressure to build up above the liquid surface; the term "empty target" is in the following understood as a target filled with cold deuterium gas. - For thermic isolation, the target had been wrapped into aluminized mylar foils which had a total thickness, together with the target wall itself, of 0.004".

In general, the target could never be seen completely by the spectrometer except for low angle settings; then the end regions of the target were seen by the outer elements of the hodoscope. Ten elements from either end of the hodoscope, however, were anyway always excluded in the data analysis because of too low counting rates.

Multiple scattering due to the whole target setup is composed from the following contributions:

a) a spreading in deuterium before He3 production,

b) " " " " after " " ,and

c) " " at entering through the vacuum chamber window (mylar), the reflecting foil, and the target wall, and at leaving through the same layers. The corresponding $\Delta\theta$ due to all three effects together shall be called $\Delta\theta_t$.

The Magnet

The magnet was operated between 8 and 16 KGauss. Being equipped with end guards, the magnet produced a field distribution that could safely be called uniform within the used volume of the gap; the variations were less than 10^{-3}.

The field strength was monitored continuously by a digital voltmeter and the fluctuations were also less

than 10^{-3}. The correct gauge of the voltmeter was obtained by checking with a Hall probe.

Essential were the focussing properties of the magnet. With wire orbit measurements, the central point of the focal plane and the tilt of the plane itself have been measured for a typical field strength.

For geometrical proportions of the magnet and the collimator inside, see fig.8 .

The Counters:

The scintillation material was consistently lucite of various thicknesses which are indicated in fig.9 . T_0 was looked at by four phototubes, one at each side of the square. The four signals were simply added as - because of the small size of the counter - , even the worst possible timing differences between the pulses resulted in no appreciable effect upon the shape and height of the total added signal. T_{1H} was being looked at by two phototubes, one at each end, and again the pulses had been added. Pulse uniformity across the whole counter was checked and found to lie between peak value (in the center of the counter) and 10% below . T_{1V} was looked at by two tubes, too; but the pulses were not added, but treated separately as T_{1U} and T_{1L}

- these are the upper and lower tubes, respectively -, because the two ends of the counter corresponded to different momentum ranges, giving appreciable timing differences. On the other hand, these timing differences had not to be equalized by a variable delay line; it was possible to insert a fixed delay cable, because the signal from the T_{1L} discriminator was made very large (30 nanosec.).- T2 was subdivided into four sections, T_{21}, T_{22} , T_{23}, and T_{24}, each having attached to itself three tubes. The three pulses from each section had been added, and after pulse height discrimination, the four sections were joined in an OR-circuitry. Similar to T_{1V}, the four pulses had a relative timing that was dependent on the chosen nominal p_{3L}. But as the pulses had to be narrow (T_2 is essential for the time-of-flight determination), the relative timing between them had to be adjusted each time that the mean value of p_{3L} was changed.

The hodoscope consisted of seventy elements of an average width of 0.276". The widths varied very slightly from element to element, resulting in a variation of efficiency. The elements were each looked at by one tube, alternatingly located at the top and at the bottom, which might produce an "odd-even" effect in the counting rates

across the hodoscope. Both effects had been investigated (see sect. 6).

Behind T_2, finally, a pulse height monitor had been installed, a lucite counter of about one third the size of the whole T_2. Its purpose was to produce a pulse height spectrum of all the events that produced a master trigger, and to present a continuous check upon how well the trigger system was tuned for He3 particles.

The Electronics:

Fig. 10 shows the main features of the circuitry. All counter signals from T_0, T_{1H}, and T_2 were treated by differential discriminators in the low-level-timing mode (LLT), in which output and input signals are separated by a fixed time interval which is almost independent of the shape and height of the input signal. After the very high rates of T_0 and T_2 had each been reduced considerably by a slow coincidence with T_{1L}, the logic signals from T_0, T_{1U}, T_{1H}, and T_2 were fed into a fast master coincidence circuit. This master coincidence determined essentially the time resolving power of the fast electronics and thus the velocity discrimination of the counter telescope.

The output from the fourfold coincidence produced a master trigger and was identified with the passage of a He3 particle with the desired momentum through the telescope (see sect.5) . It established a gating signal for the pulse height monitor M as well as for the discriminators associated with the seventy counters of the hodoscope. The output signal from these discriminators consisted of a steady D.C. level. As the gating master signal was the criterion for identification of He3, there was no need for careful pulse height selection of the hodoscope signals. The element number of the counter which had responded with a D.C. level was being converted into a seven bit digital number represented by seven D.C. levels. The information values that none, or that two or more elements responded were also represented by seven bit numbers; these data provided a rough check for proper timing of the circuitry concerning the hodoscope discriminators. They might also be used to estimate the chance coincidence rates in the hodoscope spectra and the efficiency of the detectors. Two further bits coded the information about which of the four T_2 sections responded. This was necessary as the accepted momentum bite was quite large. All this digitalized information was being read by a small computer; it accumulated and stored these data for final

readout onto paper tape, the latter being processed off-line by an IBM-360 computer for the data analysis. The whole process from producing a master trigger and reading the status of the seventy discriminators up to resetting the D.C. levels required a dead time of some 250 μsec. Hence a vetoing signal of this length was entered into the circuitry. The time delay between producing a fourfold coincidence and gating off of this same coincidence could be reduced down to roughly 10 nanosec.

5. Resolution

Contaminations:

In the reaction p + d $\longrightarrow$ He3 + MM, the He3 particles emerging from the target and passing through the magnet may be contaminated by the following charged particles: $\pi^{\pm}$, p, d, t, and He4.

The ranges of He3 momenta that are covered, are 2.1...2.5 GeV/c for the 5 GeV/c runs, and 2.8...3.7 GeV/c for the 12.33 GeV/c runs. In fig.11, the velocities (in terms of time-of-flight) and the relative pulse heights of the above mentioned particles are plotted against their momenta. Concerning the problems in selecting He3 out of all the reaction products, the worst case is given for high momentum. Taking 3.7 GeV/c as representative, the results are read off from fig.11:

Protons and pions are easily rejected by proper pulse height selection, tritons by time-of-flight selection. Deuterons have to be rejected carefully by both methods combined. All these arguments hold with a momentum bite $\Delta p/p \simeq \pm 7\%$ per T2-section and a time-of-flight resolution of ± 5 nanosec (given by the pulse widths entering the main coincidence circuit). He4 production is relatively low, as a double process is needed, e.g. p + d $\longrightarrow$ p + d and d + d $\longrightarrow$ He4 + X, or a

very rare process (phase space!) like p + d $\longrightarrow$ He4 + $\bar{n}$, and the few He4 produced are then suppressed by time-of-flight. It should be noted that all particles which are not He3 but arrive at the same angle and are bent through the same 28°, could never be produced in a single process inside the target; kinematically they have to be the result of a multiple process (c.f.fig.5).

The resultant contamination stems from pions, protons, and deuterons which produce a dE/dx that is far off the mean value and on the Landau tail. A safe estimate for the upper limit of this contamination,(which will not be detectable in the pulse height spectrum of the monitor counter M) is $\leq 10^{-4}$ (4).

As far as the He3 production itself is concerned, we get three different contributions:(a)from the liquid, (b)from the target walls and heatshield, and (c) from nuclear interactions in the counters. (c) may be completely neglected against (b) - T_0 for instance has a thickness of 6×10^{-3} collision lengths - ; (b) turned out, however, to be a serious problem of background in (a). An estimate for (b) can be obtained from (target empty rate)/(target full rate) = = (rate from (b))/(rate from (a) + rate from (b)). Therefore, at several times this ratio had been measured (sect.9)

Resolution:

The wanted observable is the missing mass spectrum of m_4. m_4 is now given uniquely as $m_4 = m_4(p_1, p_3, \theta_3)$ in the LAB-frame. Hence from the theory of propagation of errors:

$$(\Delta m_4)^2 = (\partial m_4/\partial p_1)^2 \cdot (\Delta p_1)^2 + (\partial m_4/\partial p_3)^2 \cdot (\Delta p_3)^2 + \\ + (\partial m_4/\partial \theta_3)^2 \cdot (\Delta \theta_3)^2 + \text{higher order terms.}$$

As already mentioned, $\partial m_4/\partial p_3 = 0$ at the Jacobian peak; hence the last term and the first term dominate by far over the middle one, considering that the momentum bite per T2-section (FWHM) is only $\pm 7\%$ (see sect.6) and that the momentum loss of the He3 inside the target is at the very most 1%.- $\Delta\theta_3$ is composed of a $\Delta\theta_{3h}$ as accepted per hodoscope element, of a $\Delta\theta_b$ and of a $\Delta\theta_t$ (see sect.4). Δp_1 is given by the beam conditions (sect.4) and by dE/dx within the target.

$\Delta\theta_{3h}$ is composed of the counter element size, the chromatic aberration of the focussing magnet, and the transformation of target related spherical angles into spectrometer related cartesian angles. It has been calculated with an acceptance program (sect.6); the FWHM of $\Delta\theta_{3h}$ is found to be just about the mean angular displacement from element to element, $\Delta\theta_{3h} \approx 0.045^\circ$.

$\Delta\theta_t$ can be found with the formula for multiple scattering as given e.g. in (6):

$$(\Delta\theta_t)^2 = (\Delta\theta_{proton})^2 + (\Delta\theta_{He3})^2 + (\Delta\theta_{foil})^2$$

with each $\Delta\theta = z \cdot \frac{21.2\ \text{MeV}}{p_{He3} \cdot \beta_{He3}} \sqrt{\frac{L}{L_{rad}}}$ in radians

For $\Delta\theta_{proton}$, L ≈ half the target length : $\Delta\theta_{pr.}$ = 1.8mrad at 5GeV
and 0.72mr at 12.33"

For $\Delta\theta_{He3}$, $L \approx \frac{\text{target radius}}{\sin\theta_3}$: $\Delta\theta_{He3} = \frac{2.55\ \text{mrad}}{p \cdot \beta(\text{GeV}) \cdot \sqrt{\sin\theta_3}}$

$\Delta\theta_{foil}$ may safely be neglected, because the total "foil" consisted of 0.003" of target wall and 0.001" of heatshield, which adds up to 3.5×10^{-5} radiation lengths of mylar.

$\Delta\theta_t$ is then tabulated in table 1 along with $\Delta\theta_b$ and $\Delta\theta_{3h}$ to yield a total combined $\Delta\theta_3$. It should be noted that the $\Delta\theta_t$ may very well be overestimated by using the quoted formula for values $L \not> L_{rad}$.

Δp_1 may be written as $(\Delta p_1)^2 = (\Delta p_b)^2 + (\Delta p_t)^2$.

From sect.4: $\Delta p_b/p_b = \left((\pm 3.2 \times 10^{-4})^2 + (\pm 5 \times 10^{-4})^2 \right)^{1/2}$

$= \pm 6 \times 10^{-4}$

This figure is correct for the 12.33 GeV/c runs but is very probable to be highly underestimated for the 5 GeV/c runs. The main contribution for Δm_4, however, comes from $\Delta\theta_3$, hence the effect on Δm_4 by low Δp_1 should not be very important.

Δp_t is given by(1/2target length)xdE/dx; hence:
Δp_t=10MeV, assuming minimum ionizing velocity, and thus

$$\Delta p_1 = 12.5 \text{ MeV/c for the 12.33 GeV/c runs}$$
$$= 10.5 \quad " \quad " \quad " \quad 5.0 \quad " \quad ".$$

The total Δm_4 is presented in table 1.

Systematic errors:

The most important systematic errors enter

i) in the knowledge of p_{inc}. At 12.33 GeV/c, the beam was well tuned, but at 5 GeV/c there was no means to check the stability of the mean momentum.

ii) in measuring the angular production distributions. By shifting the hodoscope only, it was made sure that no peculiar things were going on in the hodoscope; by changing the central angle setting it was made sure that bumps showing up in the spectra are not due to some reflections within the spectrometer system. Possible reflections of the incident beam could not be excluded this way; in fact, a change in the experimental setup downstream behind our target resulted in a slight change of the total production rates of about 1 SD. As far as total rates are concerned, this effect was taken care of by proper normalization of the rates, but the effect on the details of the obtained spectra is unpredictable.

iii) in measuring p_3. The mean value is given by the knowledge of the magnetic field; $\vec{B}$ was monitored in the beginning by a Hall probe, but later on measured by reading the voltage across a shunt resistor. This method is open to systematic errors. The mass distribution, however, is quite insensitive against an unprecise setting of p_3 (sect.2); only the momentum dependence of the production is affected. In fact, there are reasons to believe in a slight deviation of the mean momentum (sect.7).

THE RESULTS

6. Data Analysis

Definitions and Assumptions:

This section is devoted to show how the data have been manipulated. First I shall proceed to define the measured cross-sections; starting point is the definition:

$$(1)\qquad \frac{N}{N_0} = T_0' \times \iiint \frac{\partial^2\sigma}{\partial p_3 \partial \Omega_3}\, \gamma_1(\vec{\ell}) \times \theta_{acc}(p_3, \Omega_3, \vec{\ell}) \times \gamma_2(n)\, dp_3\, d\Omega_3\, d^3\ell$$

with:

N = observed number of He3 particles

N_0 = " " " incident protons

$T_0' = \frac{N_L \cdot \rho_0}{MW}$

N_L = Avogadro number

MW = molecular weight of deuterium

ρ_0 = (constant) density of LD_2

γ_1 = probability that a proton that has been registered by the monitors passes through the point $\vec{\ell}$ of the target.

θ_{acc} = +1 if a He3 particle, created at $\vec{\ell}$ with a momentum p_3 and emerging at an angle Ω_3 (as defined in fig.12) from the target, does geometrically fulfill the trigger requirements.

= 0 else

γ_2 = probability that a He3 with θ_{acc}=+1 will be

registered as a count in the n-th hodoscope element out of seventy.

Clearly, several assumptions will have to be made:

a) γ_2 gives the combined efficiency of the counter telescope and the hodoscope. As far as efficiency of the electronics is concerned, it is assumed to be 100%. Experimentally this is justified, because all counters operated safely in the plateau region of the diagram counting rate versus HT. Data taken during runs in which this condition was not unambiguously met had been handled separately. Hence, it suffices to regard γ_2 as a function reflecting possible fluctuations in the geometrical size of the hodoscope elements.

b) γ_1 : The length of the target, 24 inches, corresponds to 0.24 collision lengths of LD_2, taking a total cross-section estimate of 80mb = twice the nucleon-nucleon cross-section at 12 GeV/c. Thus the attenuation of the beam over the whole target length is in the range of about 20%. This should have a non neglegible effect upon the acceptance of the single elements; letting γ_1 = const = 0.9, however, means introducing an error that is much less than the errors which will be described below. And after all, this simplification means a large reduction in computation time. It should be mentioned that because of scattering, the size of the beam spot changes along the target, and the distribution describing

the spot is contained in γ_1 ;however, the slight convergence of the beam due to a downstream focal point and the spreading due to multiple scattering tend to cancel each other. In order to further simplify calculations, the three dimensional target is replaced by a line target in formula (1). The horizontal size of the beam spot gives only a second order effect, and the vertical size will be taken into account as an uncertainty in φ . Thus, γ_1 drops out as a constant that shall be absorbed into T_o': T_o=(def) $0.9*T_o'$.

c) N_o : N_o is the number of protons as registered by the monitors, but not necessarily the number arriving at the target. The difference should per def. be contained in γ_1 . This difference can have several origins:incorrect monitor gauge (because of changes of constellations upstream near UBM, the ratio UBM/Sem2 has a discontinuity at some point, being quite constant before and after that time; this renders UBM rather useless for data analysis, and only Sem2 has been used); introduction of a collimator (this was necessary for all 5 GeV/c runs,because of a halo around the beam, and for some of the 12.33 GeV/c runs); introduction and change of dead time - c.f.sect.4 - , which was noticeable as a change of N/N_o. All these effects can be reduced essentially by fitting the total rates N/N_o as function of angle to a smooth curve; this method will suppress the effect of uncertainty in

N_o on the shape of the missing mass spectrum, but it will leave a considerable uncertainty in the absolute values of production cross-section.

d) p_{inc}: Last not least, we have formally also an integration over the incident beam momentum. Similarly to b), this effect shall be neglected in the integration, but taken into account as a Δp_{inc} (introduced in sect. 5).

Phase Space and Efficiency:

Formula (1) has so far been reduced to:

$$N/N_o = T_o \iiint \frac{\partial^2\sigma}{\partial p\,\partial\Omega} \times \theta_{acc} \times \gamma_2 \times dp\, d\Omega\, d\ell$$

$$(2) \qquad \equiv (def)\ T_o \times \left\langle \frac{\partial^2\sigma}{\partial p\,\partial\Omega} \right\rangle \times \iiint_{\substack{\Delta p,\,\Delta\Omega \\ \Delta\ell = \pm 12''}} \theta_{acc}(p,\Omega,\ell) \times \varepsilon(p,\Omega) \times \gamma_2 \times dp\, d\Omega\, d\ell$$

All values for cross-sections will be calculated using the definition of $\left\langle \frac{\partial^2\sigma}{\partial p\,\partial\Omega} \right\rangle$ in (2). The integral is the phase space and ε is the uniform phase space population defined by $\varepsilon(p,\Omega) = \text{const}$, $\iint_{\Delta p,\,\Delta\Omega} \varepsilon \times dp\, d\Omega \equiv 1$

Formula (2) shall now be used for each single hodoscope element and each T2-section. The rate N is then to write as $N(\nu,\kappa)$, where ν designates the element number ($\nu = 1 \ldots 70$) and κ is given as the part of T2 that responded ($\kappa = 1 \ldots 4$). We get then the wanted cross-sections as average values labelled by ν and κ; but these values will have poor

statistics. Hence a different additional cross-section has been introduced by interpreting formula (2) for variable ν only, i.e. by summing over κ . These data will have no longer details concerning the momentum dependance, but they should show much better statistics.

The phase space integral, or simpler acceptance, shall be written as

$$A(\nu,\kappa) = \iiint \theta_{acc}(p,\Omega,\ell,\nu,\kappa) \times \varepsilon(p,\Omega)\, dp\, d\Omega\, d\ell$$

and (2) reduces to

$$(3) \qquad \frac{N(\nu,\kappa)}{N_0} = T_0 \times A(\nu,\kappa) \times \gamma_2(\nu) \times \left\langle \frac{\partial^2\sigma}{\partial p_3 \partial \Omega_3} \right\rangle \Big|_{\substack{p_3(\nu,\kappa) \\ \Omega_3(\nu,\kappa)}}$$

Because of the normalization of ε , the integral is independent of the ranges Δp and $\Delta\Omega$ as long as these include completely the region where $\theta_{acc} \not\equiv 0$.

The integral can only be solved if θ_{acc} is known; or else, the integral has to be solved by populating the phase space $\Delta p\, \Delta\Omega\, \Delta\ell$ uniformly, as demanded by the function $\varepsilon(p,\Omega)$, and then "ray-tracing". Several approaches are possible for this tracing through the magnet. I have chosen to follow the first order matrix method as described by several authors (7,8,9) The formulae that I have used are given in app.2. They are valid as long as Δp and $\Delta\Omega$ can be made small:

Treating the hodoscope as a whole, the Δp accepted per T2-section is $\pm 7\%$ with a total of $\pm 18\%$ over the whole T2 (the

ranges of Δp per T2-section overlap). Similarly, $\Delta\varphi$ per T2-section is $\pm 3^{\circ}$ and for the whole T2 $\pm 5^{\circ}$; $\Delta\theta$ for the full hodoscope is $\pm 1.5^{\circ}$. Hence, the only problem is the considerably large range Δp ; Steffen, however, pointed out(loc.cit.) that large values of Δp may still be treated with first order matrix formalism if the magnet constants - radius of curvature, focal lengths - are made momentum dependent.

$A(\nu,\kappa)$ has been calculated for various central angle settings θ_3 using a Monte Carlo method and then least-squares fitting these generated fluctuating data to a polygon, the general features of which are well understood and justified. Accuracy has been chosen such that the error in the polygon $A(\nu,\kappa)$ is less than 1/10 the statistical fluctuations in $N(\nu,\kappa)$. It should be mentioned that one may also define an acceptance in the conventional way by: $\alpha(\nu,\kappa) = A(\nu,\kappa)/\Delta\ell \cdot p(\nu,\kappa)$ and a total acceptance of our spectrometer, α , by summing over ν and κ. The values for α that have been obtained are:

θ_3	33	31	29	27	25	(degrees)
α	.7283	.7226	.7174	.7038	.6718	(10^{-3}sterad x mom.%)

Finally, one has to know the efficiencies γ_2 of the hodoscope elements; this means both the effects mentioned on p.15. A convenient way to measure γ_2 is to investigate the production of He3 from balsa wood:

$$\frac{N(\nu,\kappa)}{A(\nu,\kappa)} = f(\nu,\kappa) \times \gamma_2(\nu)$$

where the "carbon" cross-section represented by $f(\nu,\kappa)$ is assumed to vary smoothly in ν and κ . Hence, by a least-squares fit, γ_2 could be obtained to an accuracy given essentially by the errors of $A(\nu,\kappa)$ .This method relies, however, essentially upon the shape and position of the carbon target as being identical to the ones of the LD_2 target. But this was by no means guaranteed. Thus instead of using the calculated $A(\nu,\kappa)$, the raw carbon spectrum itself has been been fitted to a polygon-like shape with the geometries and the position of the piece of balsa entering as free parameters.

An investigation of the $\gamma_2(\nu)$ obtained from several balsa runs shows that no values of ν exist for which $\gamma_2(\nu)$ is consistently different from 1.0 , i.e. within statistics, no elements could be found with an efficiency different from the average for all balsa runs(!). This does not exclude the possibility of transient variations in efficiency due to temporary outer influences, e.g. humidity of the air affecting the phototube bases. But these effects are impossible to detect and have to be discarded as systematic errors.

Consequently, $\gamma_2(\nu) = 1$ will be assumed throughout.

Now we have all the tools to calculate $\left\langle \frac{\partial^2\sigma}{\partial p\,\partial\Omega} \right\rangle$

The momentum dependence is given by assigning to κ the mean momentum $p_3(\kappa)$ of the κ-th T2-section; θ_3 is obtained from the focussing properties of the spectrometer: By ray-tracing it has been found that the mean θ_3 accepted per hodoscope element changes by $0.0447^\circ = 0.78$ mrad from element to element. To this angle one has to add the central angle of the spectrometer setting to obtain θ_3. Once $\langle \frac{\partial^2\sigma}{\partial p \partial \Omega} \rangle$ has been expressed as a function of p_3 and θ_3, the obtained values can be combined from different spectrometer settings. The results of these calculations are given in the following two paragraphs.

7. 5 GeV/c Data

Figures 14 and 15 show the results of the calculations described in the last section for the 5 GeV/c runs: fig.14 for each T2-section and fig.15 as average over all T2-sections. The abscissa bins correspond each to the $\Delta\theta$ covered by three hodoscope elements, which is one half the FWHM of the total angular resolution (see table 1). The error bars that are marked in the diagrams are those due to statistics of the raw spectra only. A typical raw spectrum as it has actually been collected by the computer is given in fig.17 for the sum of the four T2-sections. The dotted lines in figs.14&15 correspond to the estimated background.

A very nice "bump" may be seen in fig 15. The total size of the bump is, after adding the four high counting bins together, about 0.86×10^{-32} cm^2; this represents the wanted production cross-section for this bump. The significance of the bump is roughly four standard deviations (SD). The center appears at $30.71^{\circ} \pm 4.45$ mrad (table 1); according to section 3, the resonance has a MM value of 775 ± 33 MeV/c^2.

Another bump is also appearing in fig.15, but only part of it falls into the covered range. Assuming that we see almost the whole bump in the diagram, then its production

cross-section is roughly 0.54 x 10^{-32} cm^2, its significance is about two SD, and its location is 32.25° ± 4.5 mrad or 530 ± 40 MeV/c^2.

For the first bump, fig.16 gives the background subtracted production.

From fig.14 one can read off the momentum dependence of the production; it is found to be rather steep. Remembering that $p(K) = p_3(1 \mp 0.027)$ for $K = 2$ and 3, and $p(K) = p_3(1 \mp 0.081)$ for $K = 1$ and 4 (sect.6), one finds at 30.5° for the background:

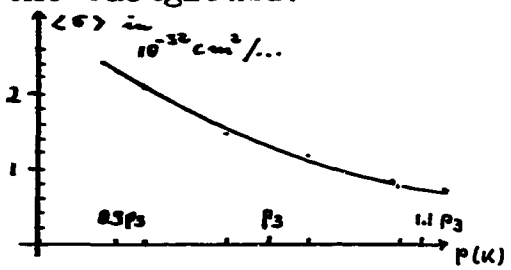

Qualitatively, this behaviour can be interpreted in terms of a multi-pion production background[11]. For the resonating production one may obtain the following estimates:

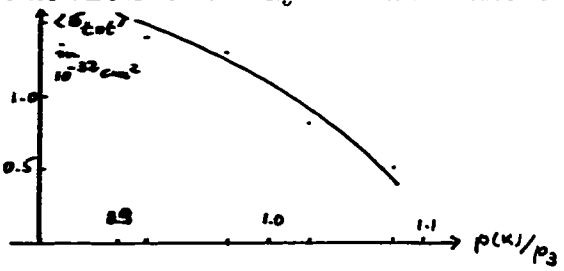

Expected is a distribution symmetric around p_3. Several explanations for this disagreement exist:a) The gauge of the magnet is off by about 1% (cf.p.24). b) Too low statistics yet. c) At the Jacobian peak, the bump would

be produced at a CMS-angle of 50° (cf.fig.5); due to true physics, the CMS angular distribution might be enhanced at smaller angles (cf.p.10), which would shift the mean momentum towards lower values.

Identification of the observed bumps:

If the structure at 32.25° is real, it is easily identified as the η meson. The resolution of $\pm$ 40 MeV/c^2 or $\pm 2.5^{\circ}$ from table 1 is in full agreement with the observed width.
The bump at 30.71° is located near the ω- and ρ- masses. The width of the ω is a fraction of the resolution, the width of the ρ is about three times as large as ΔM. Then we can say: For sure the ω is observed. The ρ, however, cannot be excluded; if it appeared, it would be too broad to be detectable. To obtain the error of the production cross-sections, an uncertainty of 10% in the monitor gauge seems appropriate (cf.p.27). Then:

$$\sigma_{tot,LAB}(\eta) \simeq 5.4 \times 10^{-3}\ \mu b \pm 12\,\%$$

$$\sigma_{tot,LAB}(\omega,\rho) \simeq 8.6 \times 10^{-3}\ \mu b \pm 16\,\%$$

8. 12 GeV/c Data

Fig. 18 shows the results for the 12.33 GeV/c runs as the analogue to fig.15: It is the average of the cross-section over the whole T2 with the bin size now chosen as 0.268° = = 4.7 mrad , which is twice the resolution. Half this bin size had been tried before without showing up any special features; hence the result is somewhat disappointing:

No resonances could be detected at 12.33 GeV/c in the chosen range of MM; the cross-section is a completely smooth function of the MM.

Then, without loss of any details, the bin size had been doubled to give fig.18. The error bars are again only due to the statistics in the raw spectra, and a typical error in the monitor gauge is again of the order of 10%. Furthermore, nothing is gained by listing the results for the single T2-sections; merely at a representative angle of 28°, the momentum dependence shall be given:

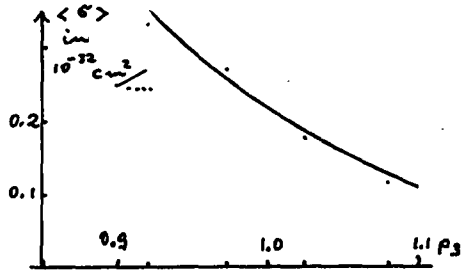

The result is similar to the 5 GeV/c data, only the momentum dependence is slightly steeper. A possible explanation for

this fact is that the process is open to a higher multiplicity of pion-production.

As for the not appearing resonances, the missing of bumps is very probably due to a very low cross-section, because from recent CERN experiments[12,13] there are several resonances established in the mass region of 2 to 3 GeV/c^2, and there is no obvious reason why they should not be produced in the present reaction except if all of these resonances would have an isospin that is higher than 1 (cf.p.5). Hence we get the result:

The total cross-section in the LAB-frame for producing resonances of mass 2.....3 GeV/c^2 in the reaction p+d--> He3+MM at p_{inc}=12.33 GeV/c and with widths that are smaller or equal to ΔM (table 1), is of the order of at most 5 x 10^{-4} μb.

9. Final Remarks

a) As the vast majority of our data is from non-resonant production, it is impossible to relate p_3 to Θ_3 in $\langle \frac{\partial^2 \sigma}{\partial p_3 \partial \Omega_3} \rangle$ because no model is available for this relation. Consequently the cross-sections could not be transformed into the CMS cross-sections nor into the invariant $\langle \frac{\partial \sigma}{\partial t} \rangle$.

b) Some estimate as to the origin of the He3 production can be given. He3 is produced mainly in three processes: 1.as background from the target walls, 2.as true He3 production from the reaction p+d--> He3+MM, and 3.as background from multiple processes with LD_2.

It is assumed that 1. and 3. are roughly independent from Θ_3. Then 1. is obtained from measuring the empty target rate (cf.p.20) with the result of ~1.0 triggers per 10^{12} protons compared to , for instance, 5.6 triggers per 10^{12} protons from a full target at 29°.

To obtain some estimate about 3., a further simplifying assumption has to be made, that this background is about twice as much as a rate of He3 (!) in a reaction p + p; this is reasonable, because at high energies the total nuclear cross-sections are roughly the sum of the single nucleonic cross-sections. That process 3. is not at all neglegible is

evident from the following: At 38^{o}, no process from 2. is allowed; yet the total target full trigger rate is 3.5×10^{-12}. Direct values for 3. had been obtained by filling the target with liquid hydrogen. The He3 trigger rate at 30.5^{o} was measured to 1.7×10^{-12}. Hence, the p-p multiple process rate is $\sim 0.7 \times 10^{-12}$. This gives an estimate for 3. :

The p-d multiple process rate is of the order of 1.5×10^{-12}. Then just 1. and 2. can already explain - within statistics - the target full rate at 38^{o}. Their sum of 2.5×10^{-12} triggers per proton is indicated as dotted line in fig.18.

c) As already mentioned, the MM spectrum in π+p--→ p+MM has recently been extended by the CERN group beyond 2.5 GeV/c^2. For further reference, see (12,13). I will merely quote the results: peaks with a significance of at least 4 SD have been observed at:

2.62 / 2.80 / 2.88 / 3.02 / 3. 08 / 3.15 / 3.45 / 3.54 GeV/c^2

Appendices

(I) see page 7

We have the laws of conservation of energy and momentum:

$$\begin{aligned} p_{1L} &= p_{3L}\cos\vartheta_{3L} + p_{4L}\cos\vartheta_{4L} \\ 0 &= p_{3L}\sin\vartheta_{3L} - p_{4L}\sin\vartheta_{4L} \\ E_{1L} + m_2 &= E_{3L} + E_{4L} \\ E_{iL}^2 &= p_{iL}^2 + m_i^2 \quad (i = 1 \ldots\ldots 4) \end{aligned} \qquad (a)$$

We have further the coordinate transformation laws:

$$\begin{aligned} p'_c \sin\vartheta_c &= p_{3L}\sin\vartheta_{3L} \\ \gamma\left(p'_c\cos\vartheta_c + \beta\cdot E_{3c}\right) &= p_{3L}\cos\vartheta_{3L} \end{aligned} \qquad (b)$$

From (b) we obtain easily equation (1) on p.8.

From (a) we get very fast the derivatives of m_4 as needed in sect.5. (a) can also be used to show the existence of a Jacobian peak angle $\Theta_{3L,JP}$: $\cos\Theta_{3L,JP} = v_{3L} / \beta$; this is, however, not very useful, as v_{3L} is itself a function of Θ_{3L}. To obtain formula (2) on p.8, it is convenient to use the invariants s,t,and u. For more details, see ref.(10) .

(II) see page 29

Following Steffen (7), one obtains the relations:

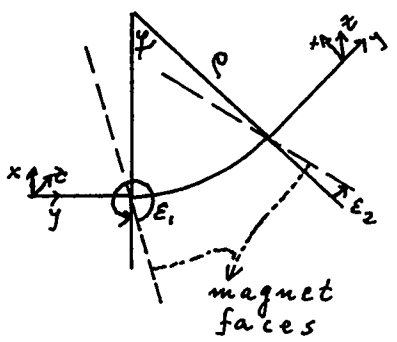

$$\begin{pmatrix} x \\ x' \end{pmatrix}_{exit} = \begin{pmatrix} 1 & 0 \\ \frac{1}{f_2} & 1 \end{pmatrix}\begin{pmatrix} \cos\varphi & \rho\sin\varphi \\ -\frac{\sin\varphi}{\rho} & \cos\varphi \end{pmatrix}\begin{pmatrix} 1 & 0 \\ \frac{1}{f_1} & 1 \end{pmatrix}\begin{pmatrix} x \\ x' \end{pmatrix}_{entrance} +$$

$$+ \left(-\frac{\Delta p}{p_0}\right)\begin{pmatrix} 1 & 0 \\ \frac{1}{f_2} & 1 \end{pmatrix}\begin{pmatrix} \rho(1-\cos\varphi) \\ \sin\varphi \end{pmatrix}$$

$$\begin{pmatrix} z \\ z' \end{pmatrix}_{exit} = \begin{pmatrix} 1 & 0 \\ -\frac{1}{f_2} & 1 \end{pmatrix}\begin{pmatrix} 1 & \rho\cdot\varphi \\ 0 & 1 \end{pmatrix}\begin{pmatrix} 1 & 0 \\ -\frac{1}{f_1} & 1 \end{pmatrix}\begin{pmatrix} z \\ z' \end{pmatrix}_{entr}$$

$$f_i = -\rho/(\delta_{corr} + \mathrm{tg}\,\varepsilon_i)$$

One recognizes the lens formulae:
The z-motion is given as a drift space of length $\rho \cdot \varphi$ sandwiched between two lenses, one at each end of the magnet. The x-motion involves also two lenses of just the negative focal strength and a drift space inbetween which, however, exerts some distortion, and a dispersion term is added.

Table (I) :

5 GeV/c:

θ_{3L}	$\Delta\theta_{pr}$	$\Delta\theta_{Mes}$	$\Delta\theta_t$	$\Delta\theta_b$	$\Delta\theta_h$	$\Delta\theta_3$	Δp_1
20	1.8	2.52	3.10	3.0	.785	4.38	10.5
25	"	2.50	3.10	"	"	4.38	"
30	"	2.60	3.16	"	"	4.43	"
35	"	2.80	3.33	"	"	4.55	"

θ_{3L}	$\Delta\theta_3$	ΔM_{ϑ_3}	Δp_1	ΔM_{p_1}	ΔM
28	4.42	26.5	10.5	2.8	26.6
30	4.43	30.1	"	3.1	30.3
32	4.47	36.7	"	4.0	36.9
34	4.51	79.0	"	6.6	79.3

12.33 GeV/c:

θ_{3L}	$\Delta\theta_{pr}$	$\Delta\theta_{Mes}$	$\Delta\theta_t$	$\Delta\theta_b$	$\Delta\theta_{Mod}$	$\Delta\theta_3$	Δp_1	ΔM_{ϑ_3}	ΔM_{p_1}	ΔM
20	.72	1.36	1.54	1.0	.785	2.00	12.5	11.0	2.5	11.3
25	"	1.41	1.58	"	"	2.03	"	14.1	2.2	14.3
30	"	1.51	1.67	"	"	2.10	"	19.2	1.9	19.3
35	"	1.68	1.83	"	"	2.23	"	32.9	1.7	32.9

Note: all angles in mrad

all masses in MeV/c^2

all momenta in MeV/c

References:

(1) Phys.Lett. 22,233

(2) Review of particle properties, UCRL-8030

(3) Phys.Rev.Lett. 21,778

(4) ZGS-Proposal for the experiment p+d--→He3+X^o, Sept.24,1968

(5) Phys.Lett. 18,185

(6) Yuan & Wu, Nuclear Physics, Vol.5, N.Y.1961

(7) K.G.Steffen, High energy beam optics, N.Y.1965

(8) Rev.of Scient.Instr. 22,717

(9) K.L.Brown, SLAC-Report No.75, July 1967

(10) G.Källén, Elementary particle physics, Reading, Mass. 1964

(11) D.G.Ryan, private communication

(12) Phys.Lett. 30,129

(13) R.Baud et al., Spectrum of charged non-strange bosons in the mass region from 3.0 to 3.8 GeV (to be published in Phys.Lett.)

fig 1

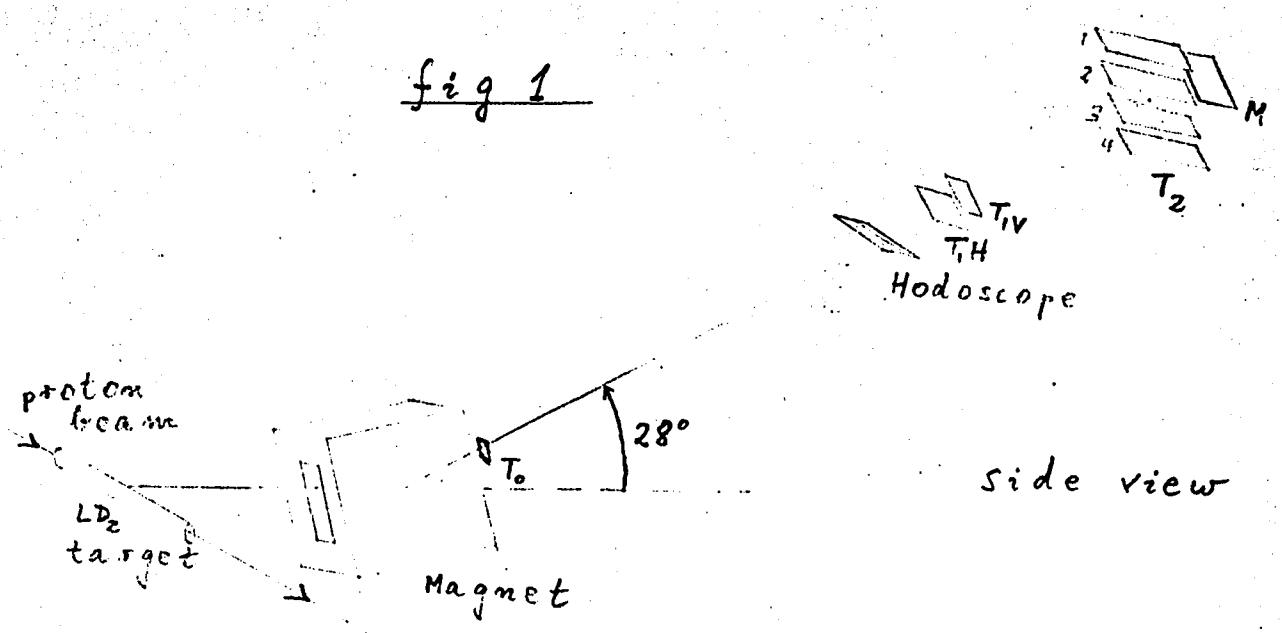
1
2
3
4
M
T2
TIV
TIH
Hodoscope
proton beam
28°
T0
LD2 target
Magnet
side view

fig 2

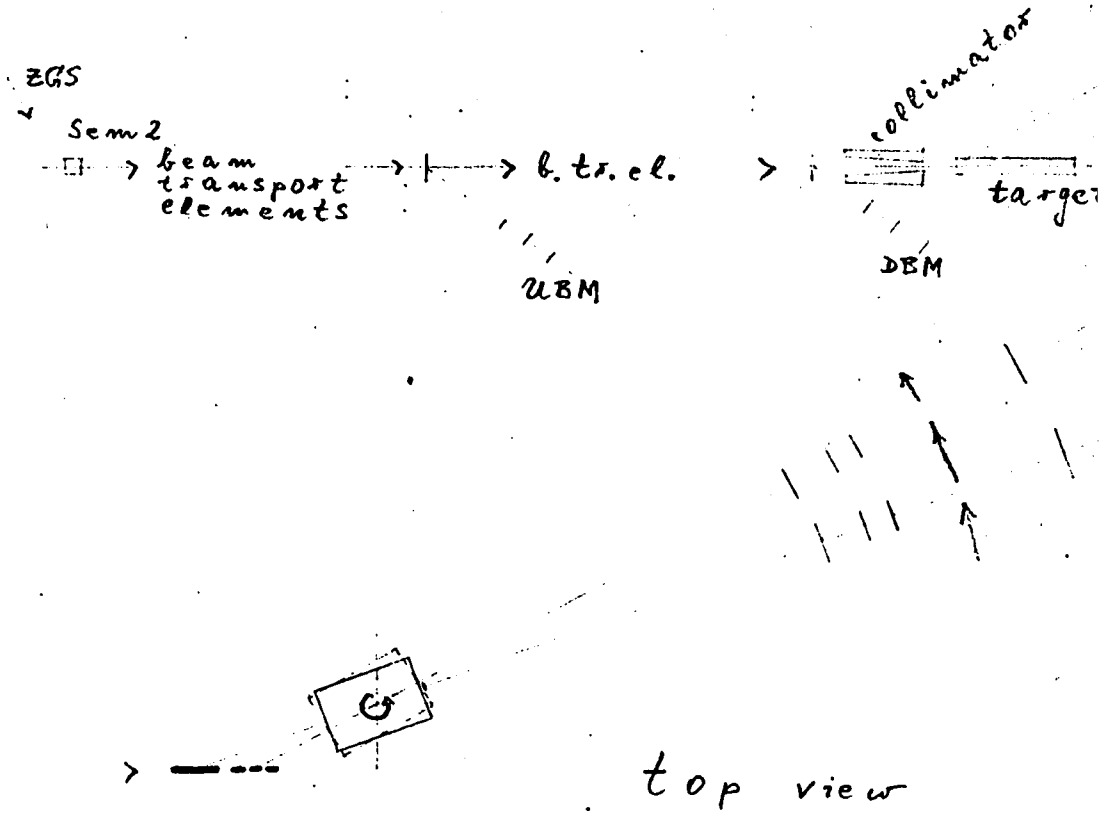
ZGS
Sem 2
beam transport elements
b. tr. el.
collimator
target
UBM
DBM
top view

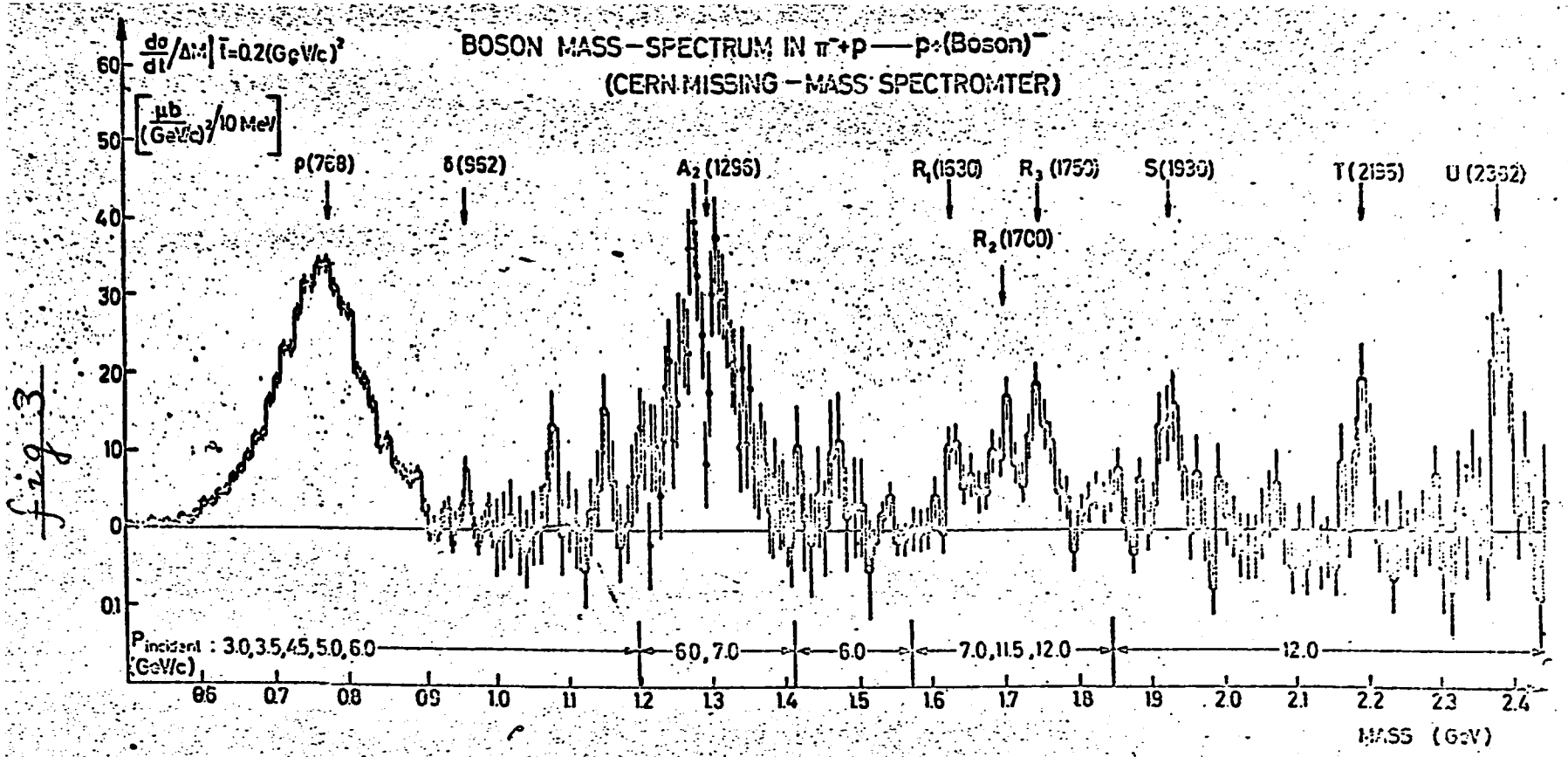

fig 3

This constitutes a copy from: W. Kienzle, Bosonic Resonances, NP Internal Report 68-25 Aug. '68, CERN.

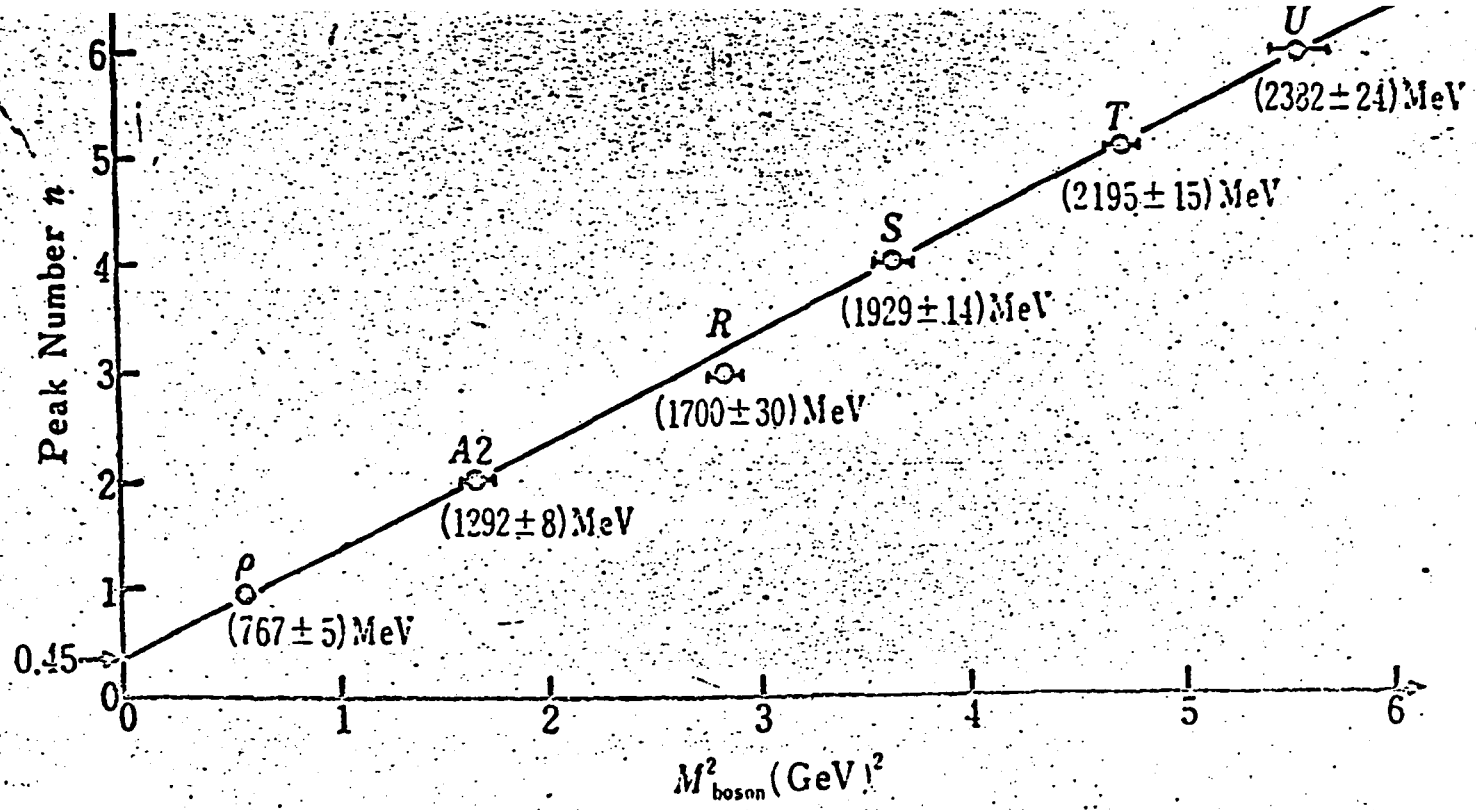

fig 4

FIG. 6. A plot of the dominant mesonic excitations observed in the reaction $\pi^- + p \to p +$ (missing mass) studied with the missing mass spectrometer by the Maglic group at CERN[45]. The peaks are numbered n in order of increasing mass, starting with the ρ-meson, and n is plotted against (mass)^2 for each mesonic excitation.

This constitutes a copy from: W. Kienzle, Boson Resonances, NP Internal Report 68-25, Aug. '68, CERN

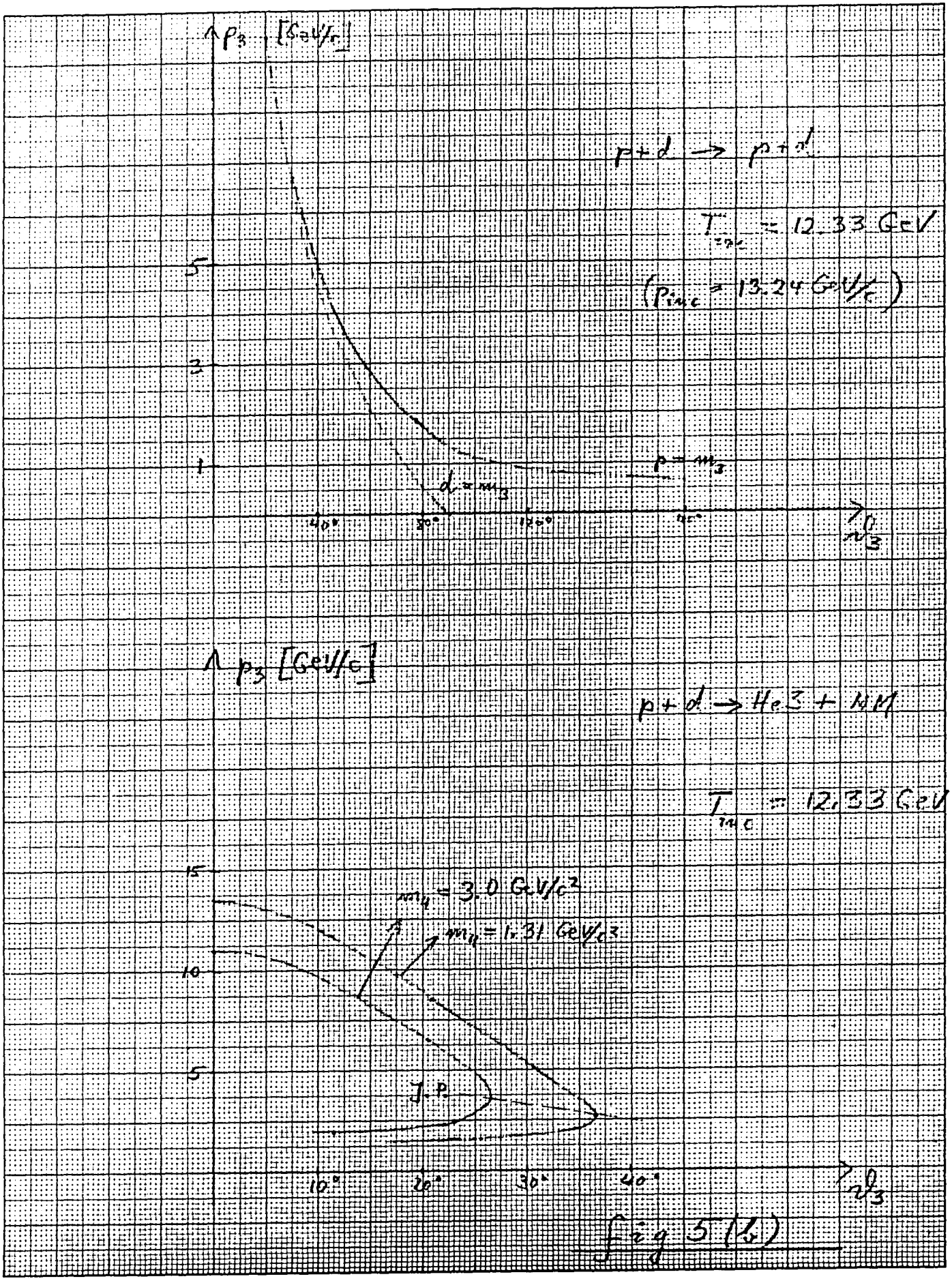

Fig 5 (1)

fig 6

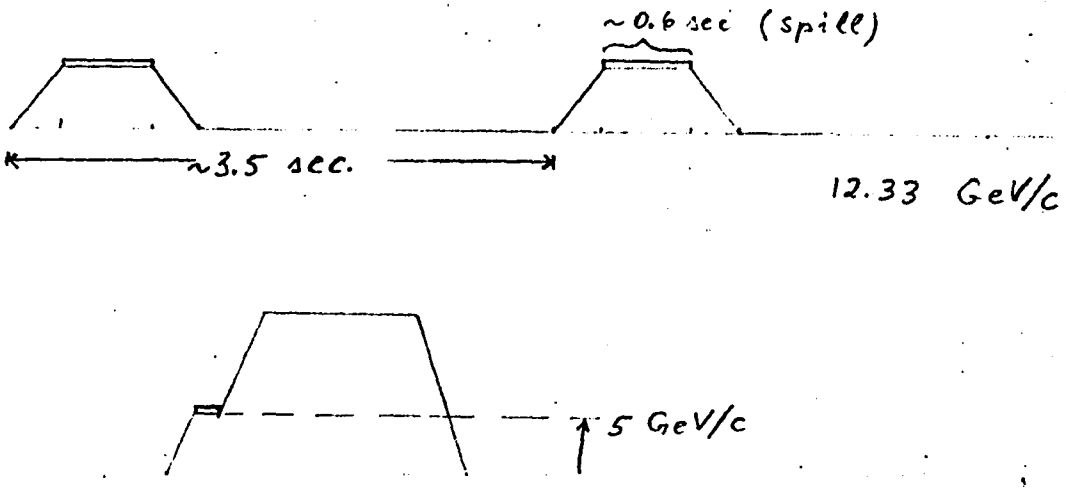

fig 7

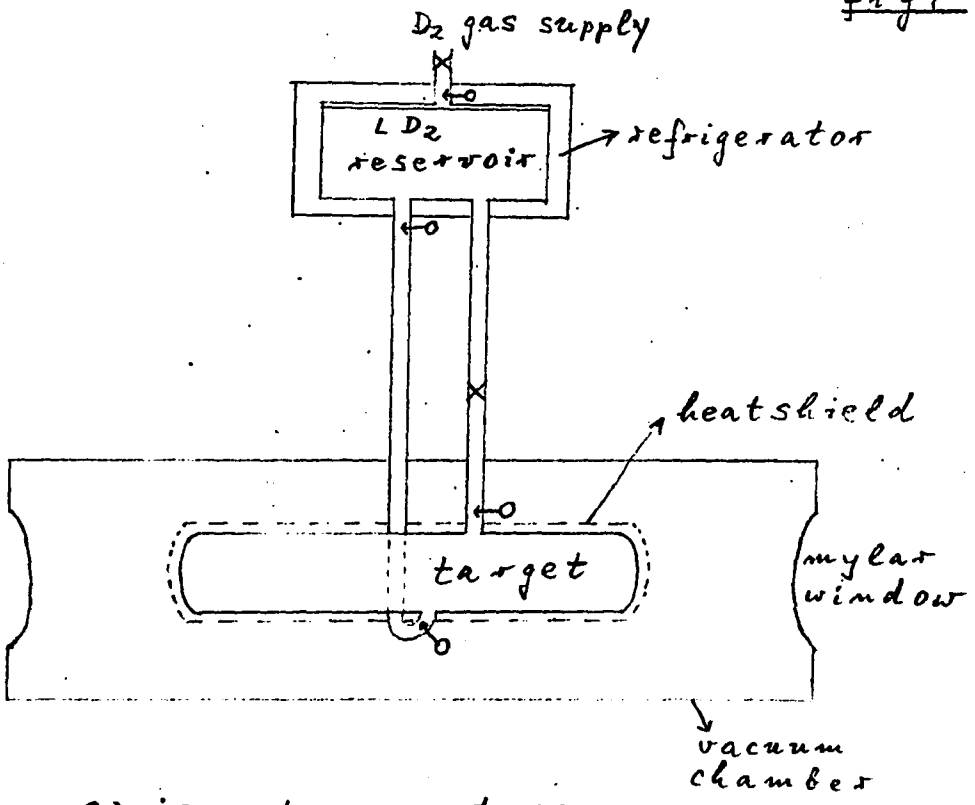

→ is a temperature sensitive resistor

fig 8

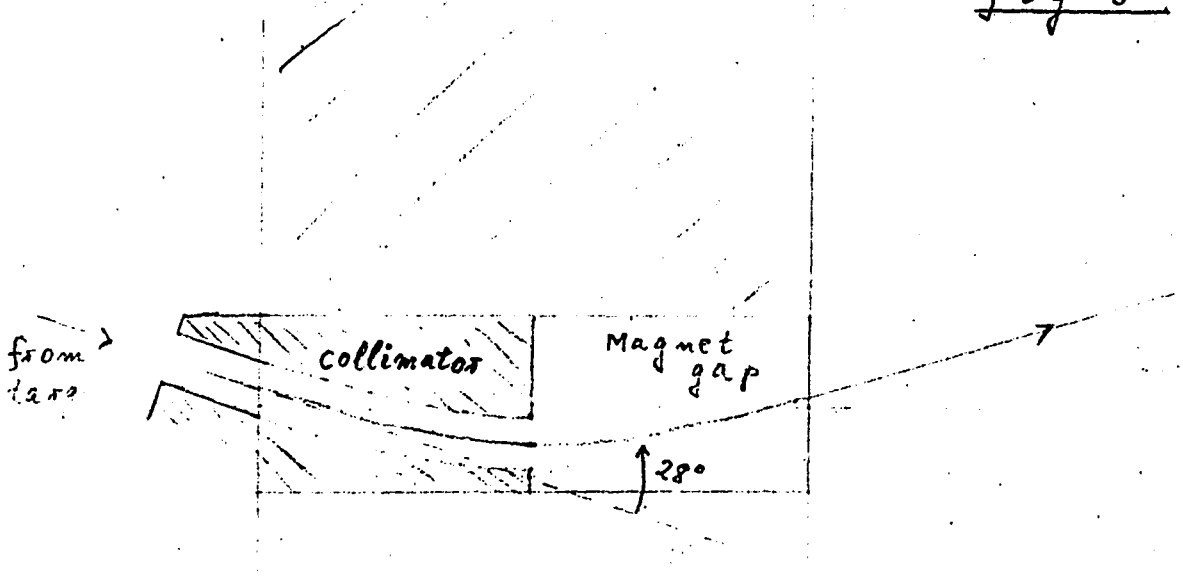

fig 9

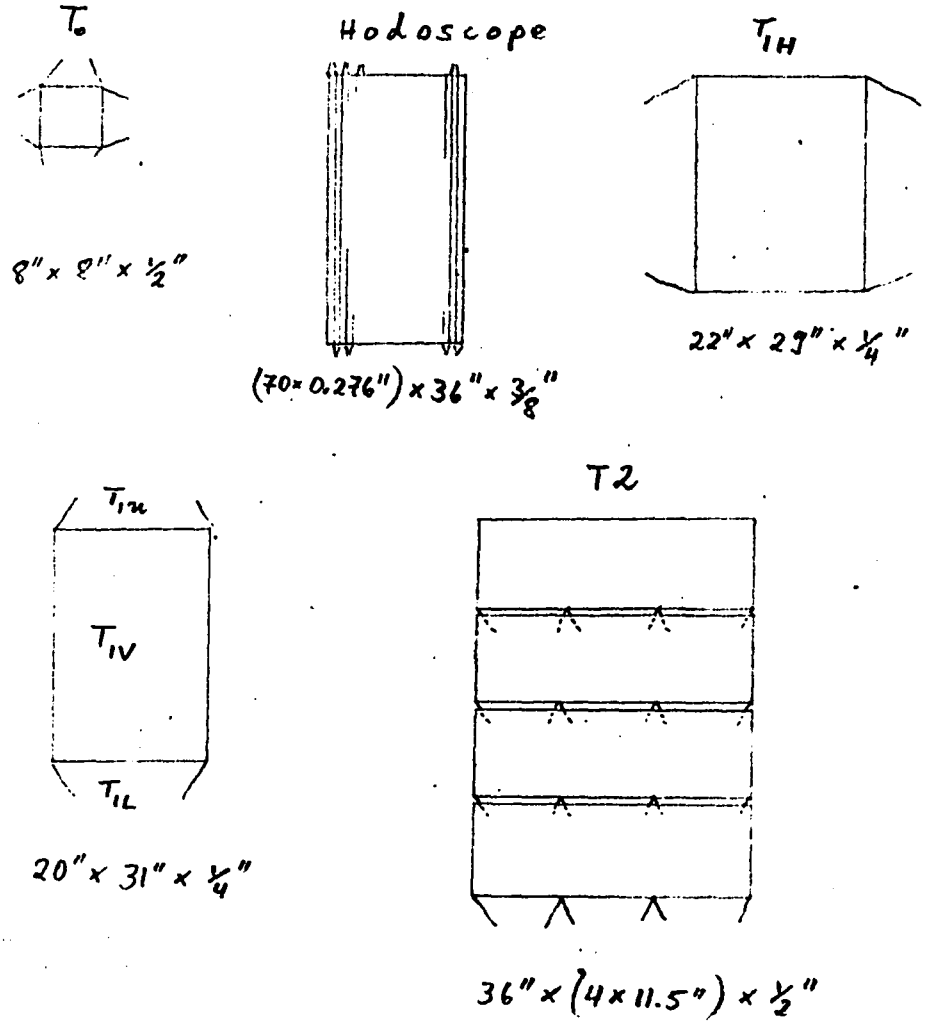

indicated are the light-guides

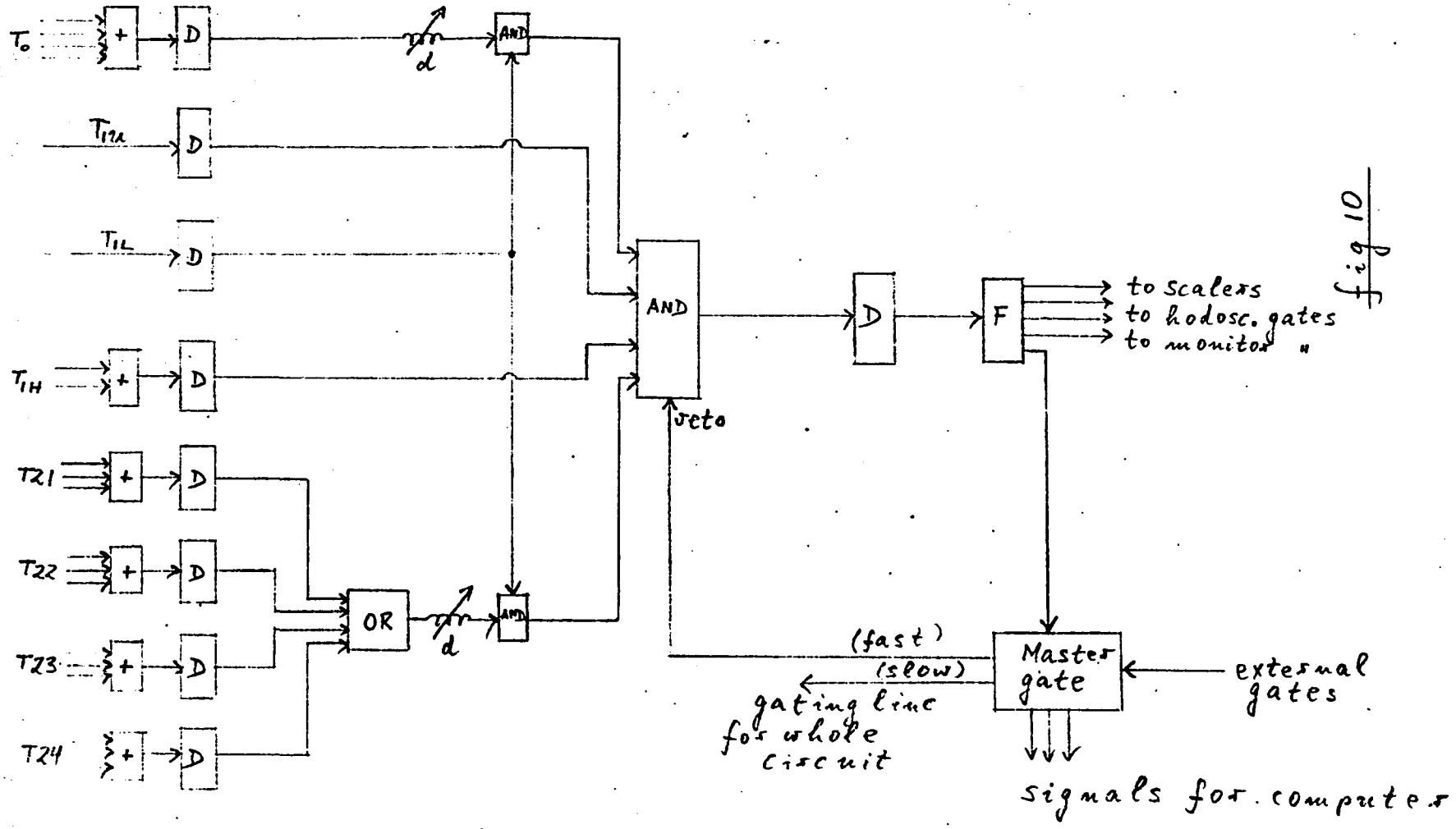

"+" : adder

"D" : discriminator

"d" : variable delay cable

fig 12

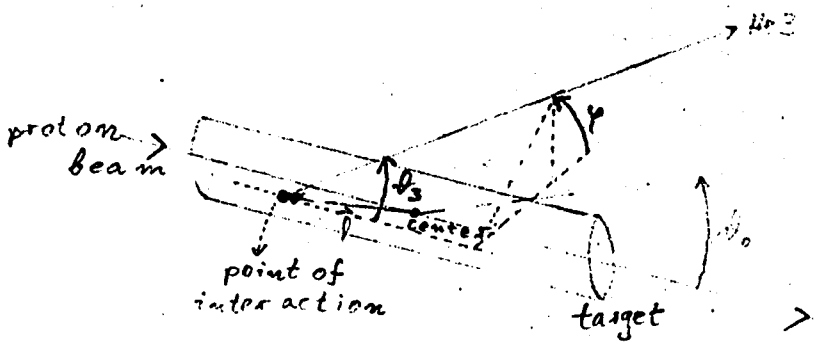

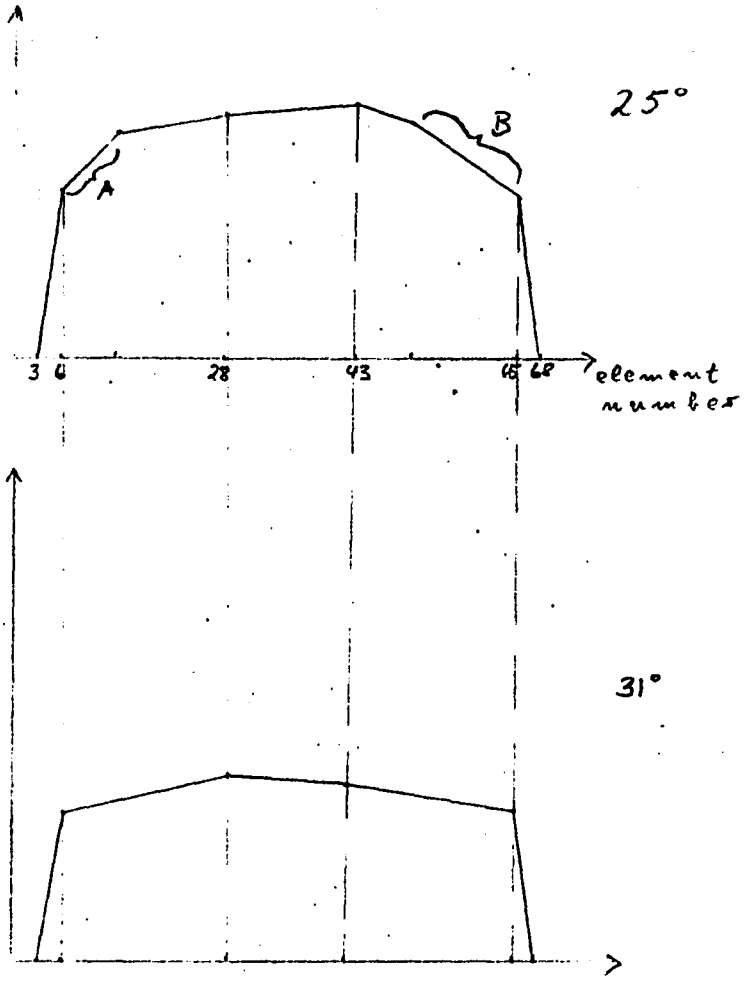

display of $A(\gamma, K=1)$ in arbitrary units

A and B represent "target ends" - effects

fig 13

fig 14

fig 15

fig 16

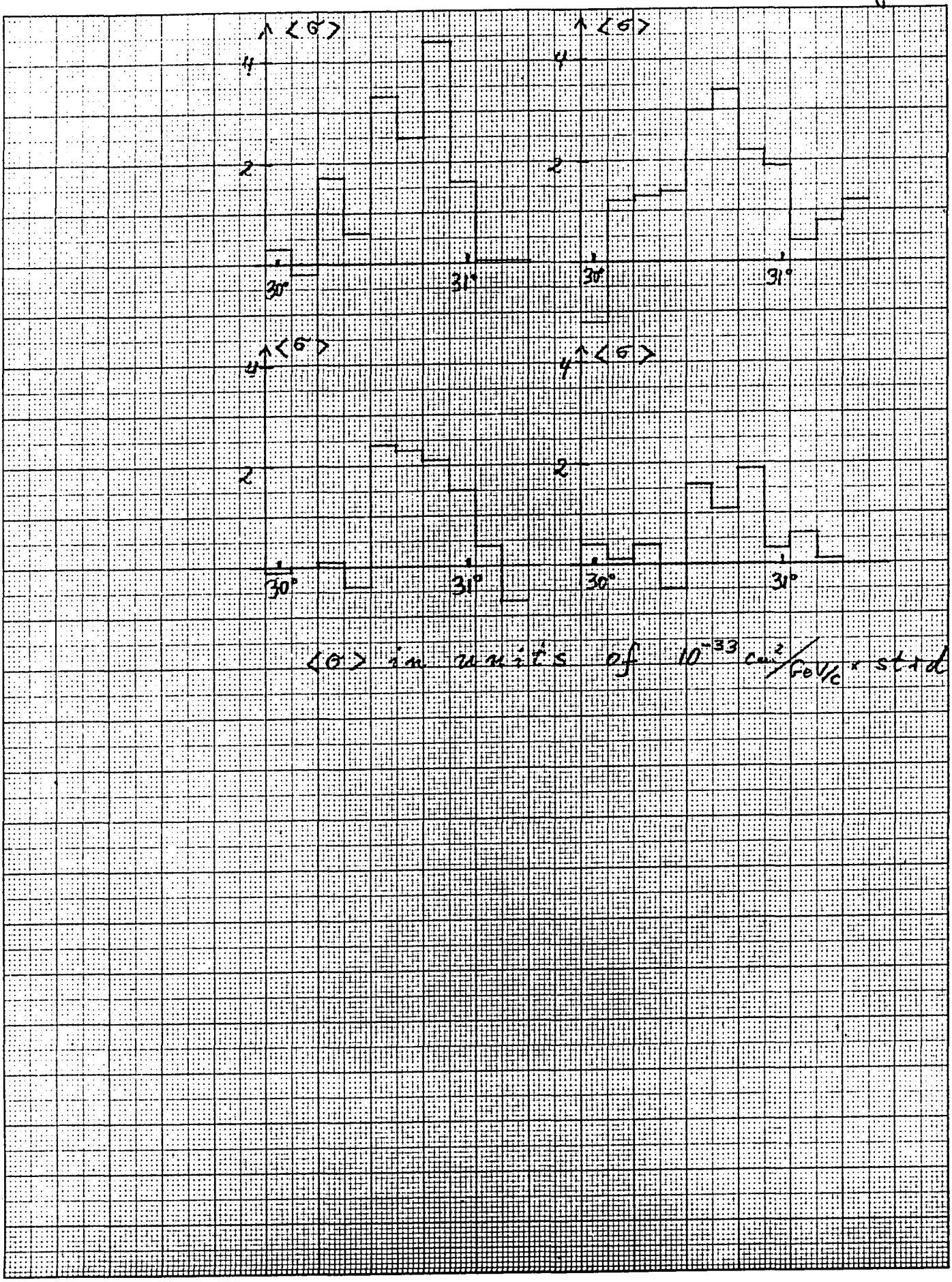

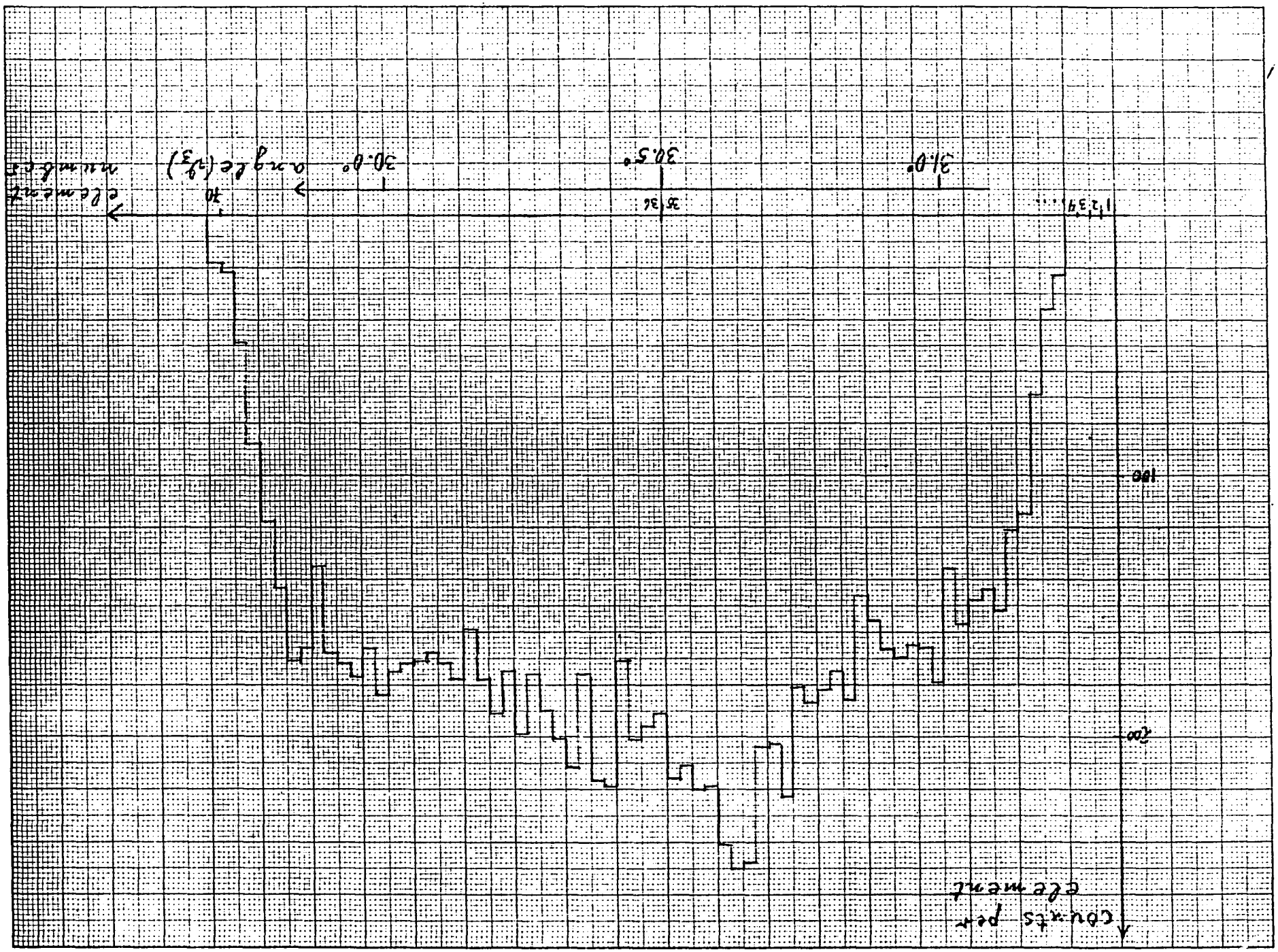

Fig 12

fig 18